Zhang et al. Chin. J. Mech. Eng. (2019) 32:48
https://doi.org/10.1186/s10033-019-0362-6

Chinese Journal of Mechanical Engineering

ORIGINAL ARTICLE

Open Access

Modified Pre-stretching Assembly Method for Cable-Driven Systems

Guokai Zhang[1,2], Xuyang Ren[1,2], Jinhua Li[1,2*], Kang Kong[1,2], Shuxin Wang[1,2] and Jingchao Shen[1,2]

Abstract

Soft cable-driven systems have been employed in many assembled mechanisms, such as industrial robots, parallel kinematic mechanism machines, medical devices, and humaniform hands. A pre-stretching process is necessary to guarantee the quality of cable-driven systems during the assembly process. However, the stress relaxation of cables becomes a critical concern during long-term operation. This study investigates the effects of non-uniform deformation and long-term stress relaxation of the driven cables owing to moving parts in the system. A simple closed-loop cable-driven system is built and an alternating load is applied to it to replicate the operation of transmission cables. Under different experimental conditions, the cable tension is recorded and the boundary data are selected to be curve-fitted. Based on the fitted results, a formula is presented to estimate the stress relaxation of cables to evaluate the assembly performance. Further experimental results show that the stress relaxation is mainly caused by cable creep and the assembly procedure. To remove the influence of the assembly procedure, a modified pre-stretching assembly method based on the stress relaxation theory is proposed and verification experiments are performed. Finally, the assembly performance is optimized using a cable-driven surgical robot as an example. This paper proposes a dual stretching method instead of the pre-stretching method to assemble the cable-driven system to improve its performance and prolong its service life.

Keywords: Performance, Cable-driven system, Pre-stretching, Assembly

1 Introduction

Assembly systems may consist of rigid components or compliant components, such as cables [1–3]. Soft cable-driven systems have been employed in many areas, such as industrial robots, parallel kinematic mechanism machines, medical devices, and humaniform hands [4–8]. The special characteristics of such systems are described as follows [4, 9–11]: a) Cables need to be subjected to a stretching force. When the stretching force decreases to zero, the cables will loosen and stop functioning. Thus, the cables must be maintained in tension throughout the assembly process; b) Cable-driven systems occupy smaller space than traditional link-driven systems, and consequently, a larger area can be available for other components; c) Owing to their flexibility, cables can transmit force in small-space and multi-curvature environments; d) Cable-driven systems are more competitive in the market owing to lighter materials and smaller inertia; e) Cables would easily result in creep and stress relaxation during long-term operation. Thus, although cables have reliable features, they have remarkable shortcomings as well, which hinder their further application.

In general, researchers have focused on the kinematics of cable transmission systems. Generally, cables are regarded as inelastic components and are used in the constant-curvature model, which can simplify the kinematics and function well in many cases [12–14]. In more sophisticated models, the physical properties of cables, such as elasticity, mass, and friction, should be considered. For example, in Camarillo's work, a cable is modeled as a spring in analyzing a cardiac catheter robot [11, 15]. Kozak et al. [16] proposed a static model of cable-driven robotic manipulators with non-negligible cable mass. Chen et al. [17] proved that the inverse transmission model with friction would help control

*Correspondence: lijinhua@tju.edu.cn
[1] Key Laboratory of Mechanism Theory and Equipment Design of Ministry of Education, Tianjin University, Tianjin 300354, China
Full list of author information is available at the end of the article

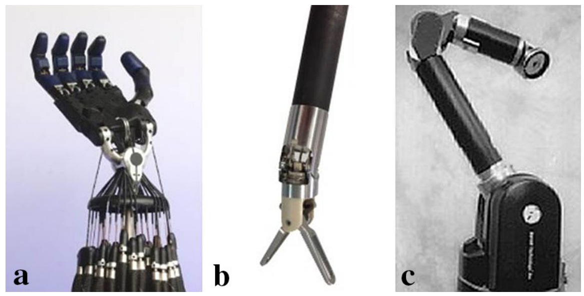

Figure 1 (**a**) Shadow Dexterous Hand (Shadow Robot Company, London, UK); (**b**) A robotic device for an invasive surgery (Tianjin University, Tianjin, China); (**c**) WMATM arm (Barrett Technology, Inc., Cambridge, Massachusetts, USA)

the displacement of a tendon–sheath transmission system without feedback.

In addition to kinematics analysis, there have been numerous studies on creep behaviors of cables to make cable-driven systems more precise and reliable [18, 19]. Guimaraes et al. conducted an experiment on the creep tests of aramid cables and proposed an empirical expression for the prediction of long-term creep [20]. Calì et al. [21] proposed an original creep prediction model with a unified comprehensive formulation and utilized the ANSYS finite element model simulations for the model validation. Kmet et al. used a modified nonlinear force-density method and a modified dynamic relaxation method to analyze the stress relaxation of cable nets [22–24]. Xu et al. [25] considered the cable assembly as a whole and proposed a creep model based on the modified Norton–Bailey equation; however, it is difficult to apply this model as it involves too many parameters. Thus, several creep and stress relaxation models have been presented, but most of them have focused on static analyses and creep models rather than dynamic analyses and stress relaxation models, which determine the working performance of cables.

In the assembly of a cable-driven system, we generally only consider the initial preload of the transmission cable as the reliable and measurable indicator for the system, but ignore the structure of the cable-driven system and complex operating conditions. Consequently, the stress relaxation of the transmission cable is unpredictable. For surgical robots and instruments, such a phenomenon may have serious consequences. Therefore, Intuitive Surgical, Inc., the company that owns the da Vinci robot-assisted surgical system, has devised strict rules for the service life of its instruments in order to enhance the safety of the entire robot system; consequently, its products are relatively expensive (Figure 1).

This study investigates the stress relaxation of cables in a cable-driven assembly and develops a solution for cable assembly using a modified pre-stretching assembly method.

2 Cable-Driven System Assembly

2.1 System Assembly

A complex cable-driven assembly may consist of many components, such as sheaves, guide pulleys, cables, and other components, as shown in Figure 2(a) [26]. It can be simplified to a typical single-loop cable-driven system composed of a master sheave, several guide pulleys, a slave sheave, and two transmission cables, as shown in Figure 2(b). The master sheave is connected to the motor, acting as the power input of the system. The slave sheave is connected to the moving parts of the system, functioning as the output. The guide pulleys change the directions of transmission to prevent the cable from interfering with other parts or being joined with the non-coplanar master and slave sheaves. Generally, two cables are connected to the master and slave sheaves to form a closed loop, which can transmit the forward and reverse driving

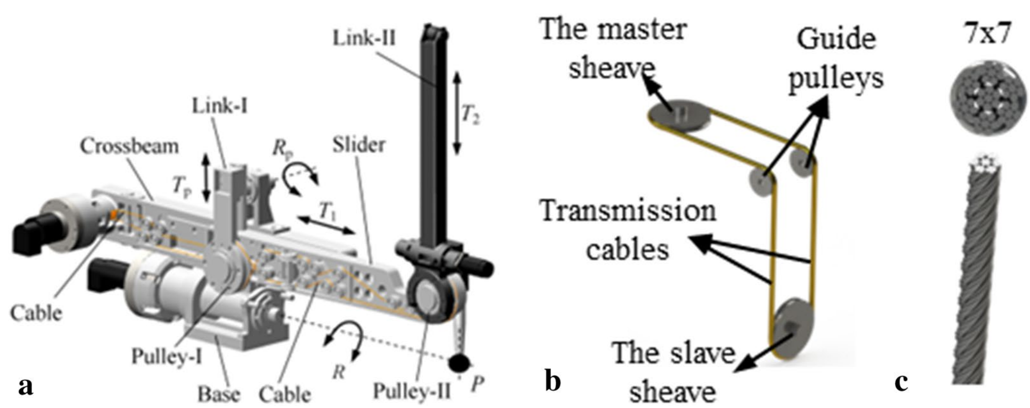

Figure 2 (**a**) Robotic arm driven by cables [8]; (**b**) Typical single-loop cable-driven transmission system; (**c**) Cable structure

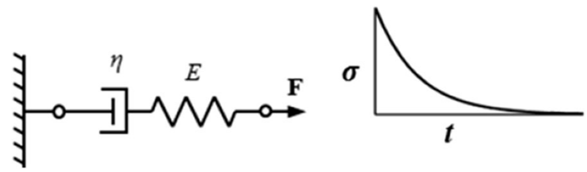

Figure 3 Maxwell model and stress relaxation curve

forces, respectively [27, 28]. If there is only one driving cable at one side, a spring-back component would be integrated at the opposite side [29]. The structure of the cable is shown in Figure 2(c). Several hairlines are twisted together tightly with very small space inside. This type of structure makes the cable flexible but can also lead to complex deformation whose model is difficult to build.

2.2 Force Analysis of Cables and the Maxwell Model

As for the transmission cable between the sheaves and pulleys, its stretching behavior is simple because it maintains pure tension. Thus, the Maxwell creep and stress relaxation model can be applied to the analysis of its stress relaxation [30, 31]. The simplest Maxwell model can be regarded as a spring-damper system as shown in Figure 3. Thus, a set of equations can be obtained:

$$\begin{cases} \dot{\varepsilon}_d = \sigma/\eta, \\ \varepsilon_s = \sigma/E, \\ \varepsilon = \varepsilon_d + \varepsilon_s, \end{cases} \tag{1}$$

where σ and ε represent the stress and strain of the model, respectively; η is the damping coefficient of the damper, E is the Young's modulus of the spring, and the subscripts d and s represent the damper and spring, respectively. Eq. (1) can be converted into a single formula as follows:

$$\dot{\varepsilon} = \frac{\sigma}{\eta} + \frac{\dot{\sigma}}{E}. \tag{2}$$

In the stress relaxation mode, the differential of the strain is equal to 0. Thus, Eq. (2) can be written as

$$\frac{\dot{\sigma}}{\sigma} = -\frac{\eta}{E}. \tag{3}$$

By integrating Eq. (3), the stress relaxation formula of the Maxwell model can be obtained as

$$\sigma(t) = \sigma_0 e^{-t/\lambda}, \tag{4}$$

where σ_0 is the initial value of stress, t is time, and $\lambda = E/\eta$ is defined as the relaxation time, which indicates that the force is reduced to $1/e$ of its initial value when t is equal to λ.

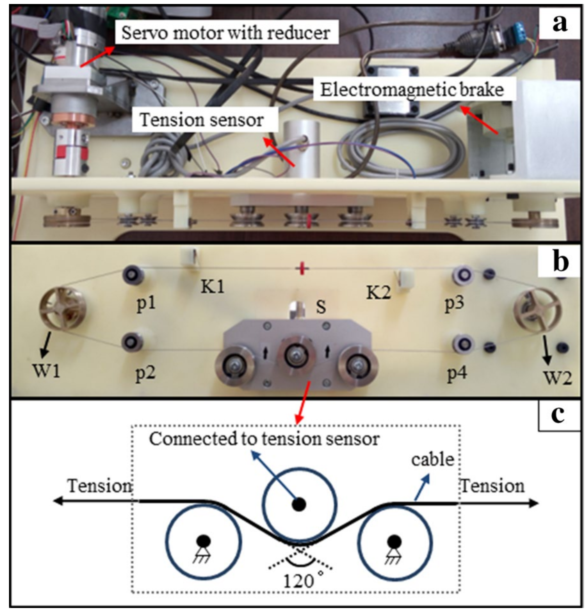

Figure 4 Experimental device: (**a**) top view; (**b**) front view; (**c**) Testing method for cable tension

When the cable is wound around the wheel, it can be influenced by the interaction of tension, pressure, friction, and inside deformation. Subsequently, the behavior of the stretching force becomes more complex and difficult to analyze. Although a theoretical creep constitutive model has been proposed in Ref. [25], it is difficult to apply as it involves many parameters. Moreover, the influence of the assembly structure and the alternating load on the cable has been neglected. Therefore, we intend to develop a modified relaxation model based on experimental data by considering the cable-driven system as a whole and replicating its motion and also to verify the law of stress relaxation.

In a cable-driven robot, the cables are generally either wound around the wheel or between the sheaves. Therefore, if a module consisting of these two types of cables is analyzed, the results could be applied to the entire robot system.

3 Experiments and Results

3.1 Experiment Setup

An experimental device has been installed to simulate the actual working environment of the cable-driven system, as shown in Figure 4(a) and (b). Herein, the master sheave W1 is connected to the servo motor; the slave sheave W2 is connected to the electromagnetic brake, which functions as the system load; p1 to p4 are the guide pulleys; K1 and K2 are used as the hard limit switches and S acts

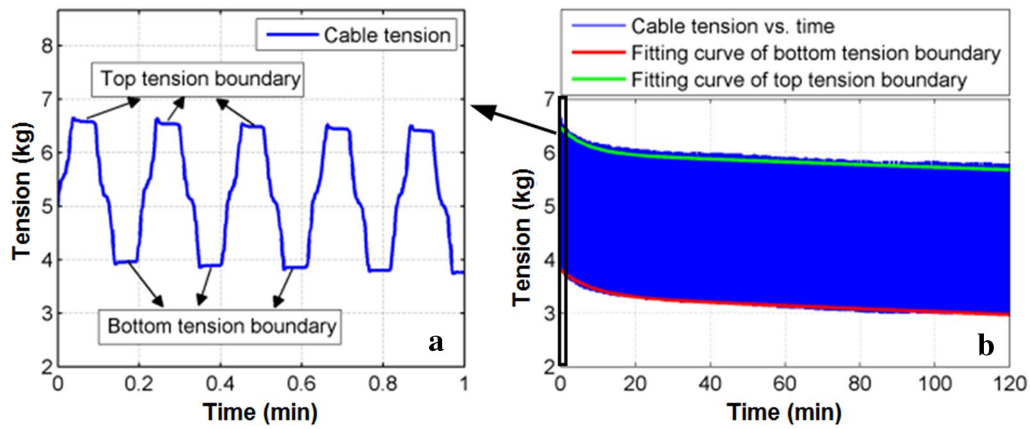

Figure 5 (**a**) Cable tension varying with the periodic motion of the experimental cable-driven assembly; (**b**) Cable tension relaxation during long-term operation and the fitting curves of the bottom and top tension boundaries

as the tension sensor. A common method for testing the cable tension is to pass the cable through three wheels as shown in Figure 4(c). When the angle between the cables on the two sides of the middle wheel is 120°, through force balance analysis it can be concluded that the normal force deployed on the middle wheel is equal to the cable tension (if the friction is ignored). The transmission cables connect W1 to W2 from upward and downward directions to form a cable loop. The electromagnetic brake can adjust the torque resistance in the range 0–4 N·m and the driving motor can provide a torque of 3 N·m. The diameters of both the drive and slave sheaves are 40 mm. The sensing precision is limited to 0.01 kg.

When the simulation system is operated, the real-time cable tension would be recorded using the tension sensor. The data would reflect the real relaxation of the cable including all the causations. Subsequently, a data-based stress relaxation formula for a cable-driven system can be derived.

3.2 Stress Relaxation under Alternating Load

3.2.1 Stress Measurements

A piece of commercial stainless-steel cable with the diameter of 0.686 mm and the maximum load of 40.8 kg is used in the experiments. According to the tension measurement, the initial preload is set to 6.0 kg. The speed of the servo motor is 30 r/min, which produces a stroke of $\pm 360°$. The load of the motor is 0.3 N·m and the test duration is 120 min. The experimental results are shown in Figure 5. Figure 5(a) displays the detailed tension change along with the periodic motion of the cable system in one minute. Although the change in tension over a short period is not of critical concern, notably, the cable bears different loads when the motor rotates in different directions. When the motor rotates in the clockwise direction, the cable below functions as an engine and bears the load torque and its tension increases rapidly; however, when the motor rotates in the counterclockwise direction, the cable becomes relaxed and the tension decreases quickly. In a movement cycle, a maximum tension and a minimum tension are generated. The maximum tension data within the test time constitute the top tension boundary and the minimum tension data constitute the bottom tension boundary. Figure 5(b) shows the cable tension caused by the long-term cyclic loading. As the time axis is compressed, the numerous blue lines shown in Figure 5(a) appear to be a contiguous blue area. It can be observed that both the top and bottom boundaries of the tension decrease with time and the drop speed decreases more quickly in the initial stage.

The top and bottom boundaries of the cable tension are modeled by using the Curve Fitting Toolbox in MATLAB (The MathWorks, Inc.). The result indicates that the stress relaxation can be described by the following function:

$$T = ae^{bt} + ce^{dt}, \tag{5}$$

where a, b, c, and d are constant parameters, t represents time, and T represents the cable tension.

We performed additional experiments with different cable diameters to verify the accuracy of Eq. (5). As indicated by the results in Figure 6, Eq. (5) satisfies the requirement of the relaxation model under the alternating load condition. The fitting parameters of the six lines in Figure 6 are listed in Table 1. Subscripts t and b represent top and bottom, respectively.

Based on the fitted parameters, it can be observed that there is a significant difference in the parameter values ($a < c$, $b >> d$), which indicates that the stress

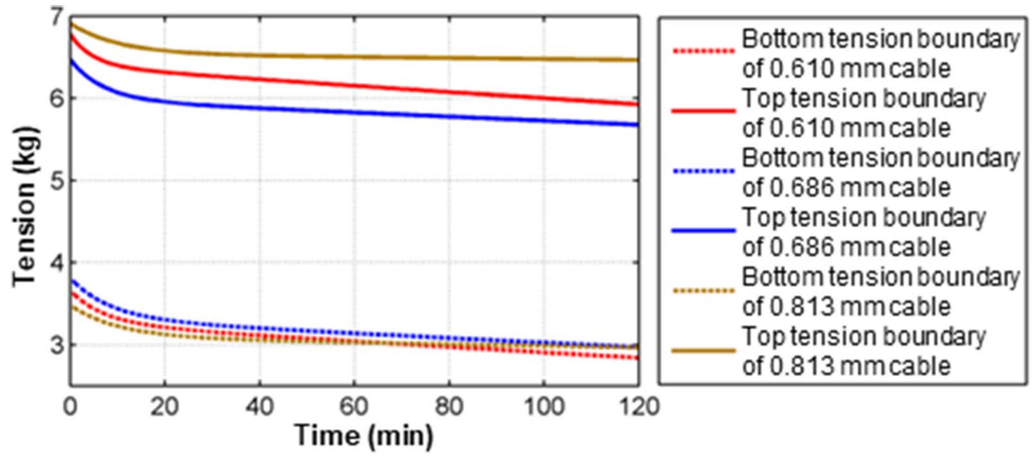

Figure 6 Fitting curves of cables of diameters 0.610, 0.686, and 0.813 mm

Table 1 Fitting parameters of the tension boundary

		Diameter (mm)		
		0.610	**0.686**	**0.813**
a	a_b	0.3949	0.4912	0.3856
	a_t	0.3852	0.4894	0.3730
b	b_b	− 0.1415	− 0.1174	− 0.0972
	b_t	− 0.2057	− 0.1439	− 0.0977
c	c_b	3.2620	3.3170	3.0930
	c_t	6.3900	5.9800	6.5370
d	d_b	-1.152×10^{-3}	-9.184×10^{-4}	-3.518×10^{-4}
	d_t	-6.289×10^{-4}	-4.328×10^{-4}	-9.061×10^{-5}
ts (min)	ts_b	9.8593	14.6534	13.5996
	ts_t	3.3925	6.5817	6.9740

Subscripts *t* and *b* represent top and bottom, respectively

ts represents the time at which T_1 decreases to 3% of T_2, which indicates that the influence of T_1 can be ignored

relaxation is influenced by different factors. To explore the contributing factors of the parameters, we divided Eq. (5) into two parts as follows:

$$\begin{cases} T_1 = ae^{bt}, \\ T_2 = ce^{dt}. \end{cases} \tag{6}$$

Considering the cable of diameter 0.686 mm as an example, its tension boundaries (blue lines in Figure 6) can be divided into four curves according to Eq. (6) as shown in Figure 7. It can be observed that the T_1 parts of the two boundaries (the blue solid and pink dotted curves) are nearly coincident with each other and present a tendency of rapid decline with time. In contrast, the T_2 parts (the green and orange curves) remain the principal residual stress of the cable and show a similar tendency of stable decline.

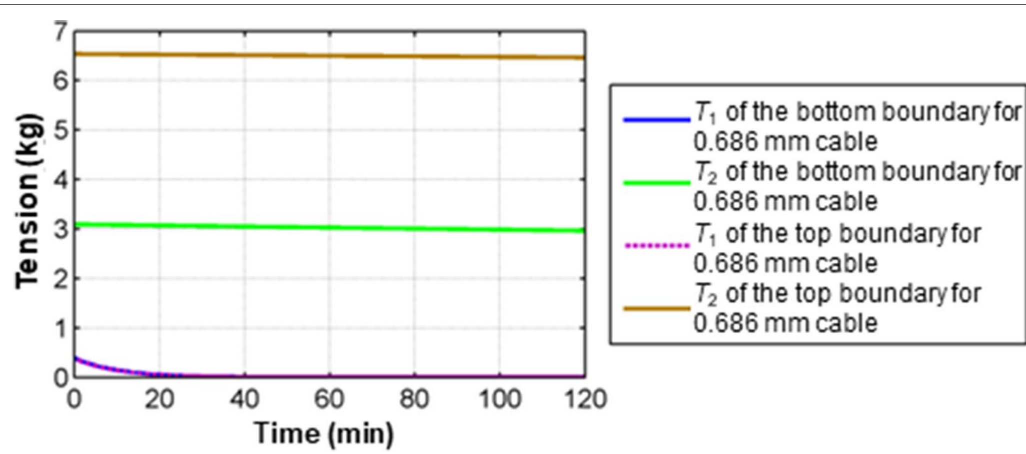

Figure 7 Boundaries of the cable of diameter 0.686 mm divided into four curves

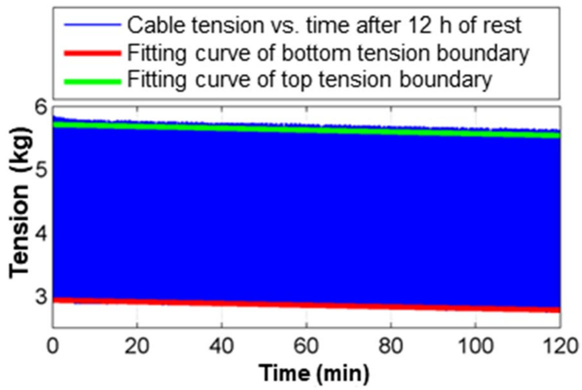

Figure 8 Cable tension relaxation vs. time after 12 h of rest and the fitting curves of the bottom and top tension boundaries

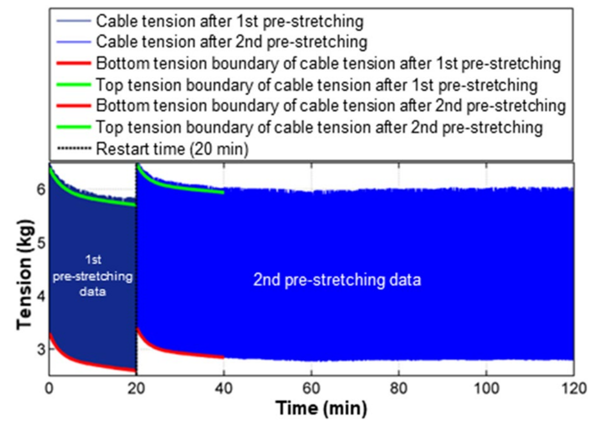

Figure 9 Tension relaxation after first and second assemblies

We have conducted comparative experiments to explore the factors influencing T_1 and T_2. As the different diameters of cables result in the same formula, we consider the cable with diameter 0.686 mm as an example to conduct the subsequent experiments.

3.2.2 Stress Measurement after 12 h

Based on the tension measurement shown in Figure 6, the experiment is stopped and the assembly is maintained in rest for 12 h. During this period, the cable is maintained in tension, and hence, it undergoes no more stretching and it does not need to be assembled for the subsequent measurement. Subsequently, we restart the experiment.

Figure 8 demonstrates the tension change and the boundaries can be fitted as follows:

$$T' = c' e^{d' t}, \tag{7}$$

and the parameters are

$$\begin{cases} c'_b = 2.937, & d'_b = -4.619 \times 10^{-4}, \\ c'_t = 5.712, & d'_t = -2.571 \times 10^{-4}. \end{cases} \tag{8}$$

According to Figure 8 and Eqs. (7) and (8), T_1 disappears but T_2 still exists. Thus, the factors contributing to T_1 have been eliminated during this period, but T_2 is not affected. Further, the relationship of T_2 versus time accords well with the Maxwell creep model, which indicates that the decrease in T_2 is caused by cable creep.

3.2.3 Stress Measurement of the Reassembled System

Although the factors contributing to T_2 are evident, those contributing to T_1 are still unknown. Thus, the following comparative experiment is conducted.

Initially, the previous experiment is repeated. According to the method described in Section 3.2.1, a piece of new cable is adopted and its stress is measured under the alternating load. When the stress reaches a steady state, the process is suspended. Subsequently, the cable is loosened and the system is reassembled at once so that the cable tension will not be influenced by other factors. The value of the pre-stretching force is set to be the same as that in the previous experiment. The tension is measured continually and the result is shown in Figure 9. It can be observed that the factor contributing to the sharp decline reappears after the reassembly, which indicates that T_1 is influenced by the assembly process.

3.3 Summary

The above experiments demonstrate that the stress relaxation is mainly due to two reasons: the system structure and assembly process (T_1) and the cable creep (T_2). Creep, which is a fundamental property of physical objects under long-term stress condition, cannot be removed. However, the creep indicates a gradual stress relaxation in the cable-driven system, which indicates that the creep will not degrade the quality of the system in a short period. However, as shown in Figure 7, T_1 will decline to zero quickly. As indicated by the parameters in Table 1, T_1 accounts for approximately 8%–15% of the total tension. Therefore, there was evident stress relaxation in the initial stage of operation of the cable-driven system using the traditional pre-stretching method, which influences the accuracy, stability, and operation time of the mechanism. Thus, we propose a dual stretching method.

4 Dual Stretching Method

4.1 Introduction of the Dual Stretching Method

From the above experiments, we have concluded that the cable tension declines quickly in the initial stage of operation owing to T_1. Thus, for a stable and long service life, T_1 ought to be eliminated. As T_1 is produced by the system structure and assembly process, it can only be eliminated by system movement. Therefore, a driving device is necessary for assembling the cable-driven systems. After the elimination of T_1, the cable tension will be decreased to a certain extent. Subsequently, we increase the cable tension to its initial preload. Without the influence of T_1, the system will operate in a good condition and its service life can be prolonged. An experiment is conducted to verify the proposed method.

Step 1: Calculate the stable time. In the experiment, the time at which T_1 accounts for 3% of T_2 is considered as the stable time, because T_1 is negligible in this case. Thus, according to Eq. (6), it can be obtained that

$$ae^{b\cdot ts} = 0.03ce^{d\cdot ts}, \tag{9}$$

where ts represents the time at which the stress becomes stable and it can be solved as

$$ts = \frac{\ln(0.03c/a)}{b-d}. \tag{10}$$

The value of ts is shown in Table 1. In a typical system, when both ts_t and ts_b become stable, the system will reach a steady status. Thus,

$$ts = \max\{ts_t\,,\, ts_b\}. \tag{11}$$

For the cable of diameter 0.686 mm in this experiment system, ts is approximately 15 min.

Step 2: Assemble the cable-driven system by using the pre-stretching method. Start the system, operate it until it reaches a steady state, and record the stress relaxation curve.

Step 3: Suspend the process for a while and stretch the cable to its initial preload again. Notably, the tension of the cable must be only increased during the process of dual stretching. If relaxation is encountered, the eliminated T_1 would appear again, which indicates failure. After the dual stretching, the system operation is restarted and the tension is recorded; the result is illustrated in Figure 10.

As indicated by the figure, the stress relaxation has been significantly improved after dual stretching, which confirms that the dual stretching method is beneficial for the stability of the cable-driven system. For devices driven by cables, it is necessary to perform a simulation experiment to eliminate the first stress relaxation before putting them to use. This can effectively improve the safety and service life of the device, which has significance in relevant areas, such as surgical robotics.

4.2 Pre-stretching Method vs. Dual Stretching Method for Cable-driven Devices

A needle holder for surgical suturing is widely used in clinical applications and it requires a large clamping force. A traditional handheld needle holder assembled with rigid components is stable and can have a long service life. However, in a minimally invasive surgical system, the instruments generally have a cable-driven system; hence, their performance is closely related to the cable stress. Thus, the needle holder exclusive to the MicroHand S robotic surgical system developed by Tianjin University has been chosen as the application target. Six such instruments are divided into two groups and are assembled using pre- and dual stretching methods, respectively. The initial clamping force of the two groups is set to 15 N and each group is required to clamp the needle 300 times. The residual clamping force is tested finally and the results are shown in Figure 11.

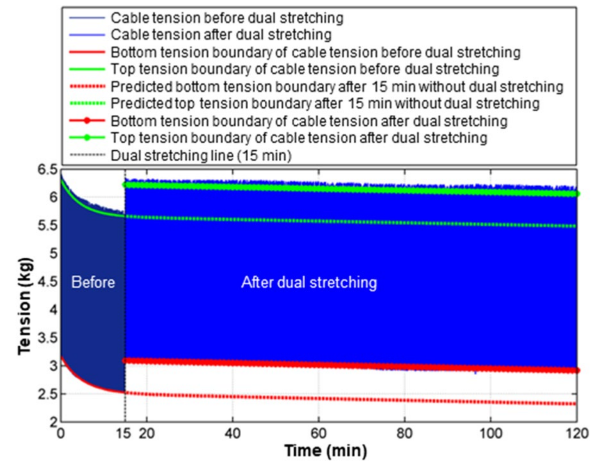

Figure 10 Tension relaxation after the dual stretching method

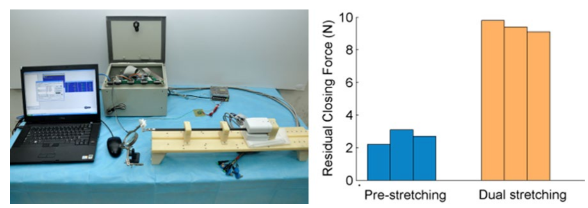

Figure 11 Pre-stretching vs. dual stretching methods for the residual clamping force test

As illustrated by the bar chart, the instruments assembled by using the dual stretching method have a higher residual clamping force even after being operated for 300 times; in contrast, the force is much smaller in the case of pre-stretching assembly.

5 Conclusions

Based on measurements and curve fitting, this paper presents a stress relaxation formula for a cable-driven assembly. Two reasons for stress relaxation have been confirmed through experiments: one is related to the system structure and assembly, and the other is attributed to the creep. To enhance the stability of the cable system, we have proposed a dual stretching method and have demonstrated its feasibility through tests. In the assembly using this method, the cable stress could be increased by 8%–15%. Considering the instruments of the MicroHand S system as an example, we have conducted a comparative study between the pre-stretching and dual stretching methods and the results prove that the needle holder assembled using the dual stretching method has a longer service life.

Authors' Contributions

JL and SW were in charge of the whole trial; GZ designed the experiments and wrote the manuscript; XR assisted with experimental setup; KK finished the comparison experiment with the needle holder; JS assisted with data analysis. All authors read and approved the final manuscript.

Author Details

[1] Key Laboratory of Mechanism Theory and Equipment Design of Ministry of Education, Tianjin University, Tianjin 300354, China. [2] School of Mechanical Engineering, Tianjin University, Tianjin 300350, China.

Authors' Information

Guokai Zhang, born in 1988, received his B.S. degree in 2011 and Ph.D. degree in 2018 both from *Department of Mechanical Engineering, Tianjin University, China*. His research interests include soft transmission system, surgical robot system and soft device.

Xuyang Ren, born in 1993, is currently a master candidate at *Department of Mechanical Engineering, Tianjin University, China.* He received his bachelor degree from *Tianjin University, China*, in 2006.

Jinhua Li, born in 1974, is currently an associate professor at *Tianjin University, China*. He received his PhD degree from *Yamaguchi University, Japan*, in 2005. His research interests include surgical robots and automation.

Kang Kong, born in 1987, received the M.S. and Ph.D. degrees in mechanical engineering from *Tianjin University, China,* in 2012 and 2017, respectively. He is currently a lecturer in the *Department of Mechanical Engineering, Tianjin University, China*. His research interest includes design and analysis of surgical robots, dexterous robotic arm and automatic control.

Shuxin Wang, born in 1966, is currently a professor at *Tianjin University, China.* He received his PhD degree from *Tianjin Universtiy, China,* in 1994. He is a Yangtze River Scholar of the Ministry of Education and the Director of *Ministry of Education Key Laboratory of Mechanism Theory and Equipment Design.* His research interest includes surgical robots, automation and multi-body dynamics.

Jingchao Shen, born in 1990, received his master degree from *Department of Mechanical Engineering, Tianjin University, China,* in 2018.

Funding

Supported by National Natural Science Foundation of China (Grant Nos. 51290293, 51520105006), and National Key R&D Program of China (Grant No. 2017YFC0110401).

Competing Interests

The authors declare that they have no competing interests.

Received: 3 December 2017 Revised: 6 December 2018 Accepted: 9 May 2019
Published online: 21 May 2019

References

[1] J Krüger, T K Lien, A Verl. Cooperation of human and machines in assembly lines. *CIRP Annals-Manufacturing Technology*, 2009, 58(2): 628–646.
[2] S J Hu, J Ko, L Weyand, et al. Assembly system design and operations for product variety. *CIRP Annals-Manufacturing Technology*, 2011, 60(2): 715–733.
[3] K W Chase, A R Parkinson. A survey of research in the application of tolerance analysis to the design of mechanical assemblies. *Research in Engineering Design*, 1991, 3(1): 23–37.
[4] B Zi, Y Li. Conclusions in theory and practice for advancing the applications of cable-driven mechanisms. *Chinese Journal of Mechanical Engineering*, 2017, 30(4): 763–765.
[5] B Ouyang, W Shang. Wrench-feasible workspace based optimization of the fixed and moving platforms for cable-driven parallel manipulators. *Robotics and Computer-Integrated Manufacturing*, 2014, 30(6): 629–635.
[6] B Ouyang, W W Shang. A new computation method for the force-closure workspace of cable-driven parallel manipulators. *Robotica*, 2015, 33(3): 537–547.
[7] G Palli, G Borghesan, C Melchiorri. Modeling, identification, and control of tendon-based actuation systems. *IEEE Transactions on Robotics*, 2012, 28(2): 277–290.
[8] S Qian, B Zi, W W Shang, et al. A review on cable-driven parallel robots. *Chinese Journal of Mechanical Engineering*, 2018, 31(1): 66.
[9] S Behzadipour, A Khajepour. Design of reduced dof parallel cable-based robots. *Mechanism and Machine Theory*, 2004, 39(10): 1051–1065.
[10] P Qi, H Liu, L Seneviratne, et al. Towards kinematic modeling of a multi-DOF tendon driven robotic catheter. *Engineering in Medicine and Biology Society (EMBC), 2014 36th Annual International Conference of the IEEE,* IEEE, 2014: 3009–3012.
[11] D B Camarillo. *Mechanics and control of tendon driven continuum manipulators*. Stanford University, 2008.
[12] R J Webster III, B A Jones. Design and kinematic modeling of constant curvature continuum robots: A review. *The International Journal of Robotics Research*, 2010, 29(13): 1661–1683.
[13] D B Camarillo, C R Carlson, J K Salisbury. Configuration tracking for continuum manipulators with coupled tendon drive. *IEEE Transactions on Robotics*, 2009, 25(4): 798–808.
[14] G Chen, M T Pham, T Redarce. Development and kinematic analysis of a silicone-rubber bending tip for colonoscopy. *2006 IEEE/RSJ International Conference on Intelligent Robots and Systems*, IEEE, 2006: 168–173.
[15] D B Camarillo, C F Milne, C R Carlson, et al. Mechanics modeling of tendon-driven continuum manipulators. *IEEE Transactions on Robotics*, 2008, 24(6): 1262–1273.
[16] K Kozak, Q Zhou, J Wang. Static analysis of cable-driven manipulators with non-negligible cable mass. *IEEE Transactions on Robotics*, 2006, 22(3): 425–433.
[17] L Chen, X Wang, W L Xu. Inverse transmission model and compensation control of a single-tendon–sheath actuator. *IEEE Transactions on Industrial Electronics*, 2014, 61(3): 1424–1433.
[18] A Zhang, L Wu. Study on the thermal creep strain property of prestress steel wire and stranded wire. *Steel Construction*, 2008, 23(1): 6–9. (in Chinese)
[19] J F Carbonell-Márquez, R Jurado-Piña, L M Gil-Martín, et al. Symmetry preserving in topological mapping for tension structures. *Engineering Structures*, 2013, 52: 64–68.
[20] G B Guimaraes, C J Burgoyne. Creep behaviour of a parallel-lay aramid rope. *Journal of Materials Science*, 1992, 27(9): 2473–2489.
[21] C Calì, G Cricrì, M Perrella. An advanced creep model allowing for hardening and damage effects. *Strain*, 2010, 46(4): 347–357.
[22] S Kmet, M Mojdis. Time-dependent analysis of cable nets using a modified nonlinear force-density method and creep theory. *Computers & Structures*, 2015, 148: 45–62.
[23] S Kmet, M Mojdis. Time-dependent analysis of cable domes using a modified dynamic relaxation method and creep theory. *Computers & Structures*, 2013, 125: 11–22.
[24] S Kmet, M Tomko, J Brda. Time-dependent analysis and simulation-based reliability assessment of suspended cables with rheological properties. *Advances in Engineering Software*, 2007, 38(8–9): 561–575.

[25] C T Xu, J G Li, Y X Yao, et al. Study of the rope nonlinear creep behaviors and its influencing factors in the assembly of sheave drives. *Mechanics of Time-Dependent Materials*, 2015, 19(3): 263–275.
[26] J Li, S Wang, X Wang, et al. Optimization of a novel mechanism for a minimally invasive surgery robot. *The International Journal of Medical Robotics and Computer Assisted Surgery*, 2010, 6(1): 83–90.
[27] C He, S Wang, Y Xing, et al. Kinematics analysis of the coupled tendon-driven robot based on the product-of-exponentials formula. *Mechanism and Machine Theory*, 2013, 60: 90–111.
[28] S L Chang, J J Lee, H C Yen. Kinematic and compliance analysis for tendon-driven robotic mechanisms with flexible tendons. *Mechanism and Machine Theory*, 2005, 40(6): 728–739.
[29] R Ozawa, H Kobayashi, K Hashirii. Analysis, classification, and design of tendon-driven mechanisms. *IEEE transactions on Robotics*, 2014, 30(2): 396–410.
[30] N W Tschoegl. *The phenomenological theory of linear viscoelastic behavior: an introduction*. Springer Science & Business Media, 2012.
[31] F Wu, J F Liu, J Wang. An improved Maxwell creep model for rock based on variable-order fractional derivatives. *Environmental Earth Sciences*, 2015, 73(11): 6965–6971.